Photoacoustics 30 (2023) 100485

Contents lists available at ScienceDirect

Photoacoustics

journal homepage: www.elsevier.com/locate/pacs

In vivo photoacoustic monitoring of vasoconstriction induced by acute hyperglycemia

Joongho Ahn [a,1], Jin Woo Baik [a,1], Donggyu Kim [a], Karam Choi [b], Seunghyun Lee [a], Sung-Min Park [a], Jin Young Kim [a], Sung Hyun Nam [b,*], Chulhong Kim [a,*]

[a] Departments of Electrical Engineering, Convergence IT Engineering, Mechanical Engineering, and Medical Science and Engineering, and Medical Device Innovation Center, Pohang University of Science and Technology, Pohang 37673, Republic of Korea
[b] Samsung Advanced Institute of Technology, Samsung Electronics Co. Ltd., Suwon 16678, Republic of Korea

ARTICLE INFO

Keywords:
Acute hyperglycemia
Endothelial dysfunction
Vasoconstriction
Intraperitoneal glucose tolerance test
Photoacoustic imaging

ABSTRACT

Postprandial hyperglycemia, blood glucose spikes, induces endothelial dysfunction, increasing cardiovascular risks. Endothelial dysfunction leads to vasoconstriction, and observation of this phenomenon is important for understanding acute hyperglycemia. However, high-resolution imaging of microvessels during acute hyperglycemia has not been fully developed. Here, we demonstrate that photoacoustic microscopy can noninvasively monitor morphological changes in blood vessels of live animals' extremities when blood glucose rises rapidly. As blood glucose level rose from 100 to 400 mg/dL following intraperitoneal glucose injection, heart/breath rate, and body temperature remained constant, but arterioles constricted by approximately –5.7 ± 1.1% within 20 min, and gradually recovered for another 40 min. In contrast, venular diameters remained within about 0.6 ± 1.5% during arteriolar constriction. Our results experimentally and statistically demonstrate that acute hyperglycemia produces transitory vasoconstriction in arterioles, with an opposite trend of change in blood glucose. These findings could help understanding vascular glucose homeostasis and the relationship between diabetes and cardiovascular diseases.

1. Introduction

Diabetes mellitus and cardiovascular diseases (CVDs) are pathologically linked [1,2]. CVDs, the most prevalent causes of death in diabetic patients due to secondary physiological disorders resulting from hyperglycemia, a condition of abnormally high glucose level in blood [3]. Recent studies have consistently found that postprandial hyperglycemia (PPH) — acute hyperglycemia following a meal — better predicts CVD events than fasting hyperglycemia [4,5]. Acute hyperglycemia causes such cardiovascular problems as high blood pressure, prolonged heart rate-adjusted QT in electrocardiograms, vascular damage, and platelet hyperaggregability [6–10]. In PPH, blood glucose spikes following a meal induce oxidative stress, endothelial dysfunction, and inflammatory reactions, leading to increased risk for cardiovascular events [4]. Further, an oscillating blood glucose level, with repeated spikes and crashes, has deleterious effects on endothelial function and causes oxidative stress [11]. Because cardiovascular risks increase with blood glucose variability, research has sought not only the mechanism by which PPH causes cardiovascular risk but also ways to predict PPH and determine the timing of insulin administration.

Vascular endothelial cells (ECs) and vascular smooth muscle cells (VSMCs) are endocrine regulators of blood flow and vascular homeostasis [12]. ECs form layers on the inner wall of blood vessels and selectively deliver molecules and hormones from blood to tissues. VSMCs modulate vascular diameters by competing vasodilation and vasoconstriction. The vascular diameters are regulated by the interaction between nitric oxide (NO) and endothelin-1 (ET-1), which are secreted on ECs and act as vasodilators and vasoconstrictors, respectively [13]. By lowering blood glucose in hyperglycemic conditions, insulin can promote either NO-mediated vasodilation or ET-1-mediated vasoconstriction [14,15]. Insulin resistance and hyperinsulinemia, however, induce endothelial dysfunction that contributes to increase NO degradation and enhanced ET-1 release, thus leading to vasoconstriction [16]. Additionally, accentuated ET-1 secretion caused by hyperglycemia and hyperinsulinemia can cause insulin resistance, which disrupts vascular glucose homeostasis, potentially damaging vascular walls and

* Corresponding authors.
E-mail addresses: sh303.nam@samsung.com (S.H. Nam), chulhong@postech.edu (C. Kim).
[1] Equal contribution

https://doi.org/10.1016/j.pacs.2023.100485
Received 14 October 2022; Received in revised form 19 March 2023; Accepted 29 March 2023
Available online 30 March 2023

increasing cardiovascular risks [17,18].

To observe the short-term changes in blood vessels during acute hyperglycemia, fast techniques are needed to capture blood vessel images. Fundus photography has been used to monitor the changes in retinal blood vessel diameters during acute hyperglycemia. After infusing dextrose and rapidly acting insulin sequentially with a certain timer interval, Bucca et al., monitored retinal vessel diameters in type-1 diabetes at 30-minute intervals, mapping the relationship between changes in blood glucose and arteriolar diameters [19]. However, neuroretinal and endothelial effects were not separated in their results, and no statistical measurements were provided. Kappelgaard et al., reported that retinal vessel dilation in type-2 diabetes was impaired on dark adaptation in the hyperglycemic state by oral glucose intake [20]. In addition, using optical coherence tomography angiography (OCTA), Kwan et al., monitored retinal blood vessel density changes in healthy subjects during acute hyperglycemia, during dark to light transition [21]. However, the use of OCTA images for quantitative studies is limited because stochastic analyses of blood vessels based on the variation of the OCTA signals are affected by blood flow, motion artifacts, and/or imaging parameters [22,23]. More importantly, although optical imaging of eyes is a good way to observe vascular response, the light exposure for the optical imaging itself may neurologically affect retinal vessel diameters. Therefore, it is difficult to distinguish between neuroretinal and endothelial effects [24]. As an another example of fast vessel imaging, laser speckle imaging (LSI) was used to monitor the change in cerebral blood flow in rats' brains during acute hyperglycemia [25]. However, it is difficult to directly visualize blood vessels and observe their morphological changes with LSI, because it represents the spatiotemporal dynamics of blood flow and tissue perfusion by capturing intensity variations among moving scattering particles. Still another fast imaging approach, flow-mediated vasodilation (FMD) assessment, measures changes in the lumen diameter of the brachial artery during reactive hyperemia. FMD is based on ultrasound (US) Doppler imaging and is clinically used to evaluate endothelial-dependent responses [26]. However, FMD's relatively poor imaging resolution and low sensitivity to blood flow changes make it useful for only large blood vessels with temporary arterial occlusion.

In comparison, photoacoustic (PA) imaging (PAI) is a good alternative for fast, high-resolution vascular imaging. The PA imaging is based on PA effect that optically irradiated target generates US waves through multiple energy conversions by light absorption, temperature rise, thermal expansion, and vibration [27–29]. This modality basically collects the US waves generated when targeted materials absorb pulsed light energy, then reconstructs them in image forms [30–32]. Fortunately, hemoglobin, an endogenous chromophore in the body, significantly absorbs light in the visible and near-infrared optical regions, enabling the PA imaging to non-invasively visualize blood vessels without any ionizing radiation or exogenous contrast agent [33–37]. PAI has been widely used in various preclinical and clinical applications [38–44]. Krumholz e. al., monitored the blood vessels in streptozotocin-induced diabetic mice weekly for 6 weeks [45]. However, they reported that the decreased vascular diameter in the chronic hyperglycemia was related to possible occlusion due to vascular damage and polyuria, not to physiological changes related to the acute hyperglycemia and its vascular responses.

Our study sought to determine whether vasoconstriction in rats in controlled experimental environments is caused by acute hyperglycemia, and further, to investigate how much and for how long the blood vessels constrict. To catch small vascular changes, we used high-resolution, high-speed PA microscopy (PAM), chosen for its high spatial and temporal resolutions [46–52]. To control other physiological parameters, devices to measure the heart rate, breath rate, and body temperature were integrated with the PAM system. To induce acute hyperglycemia, 10 normal rats were intraperitoneally injected with glucose solution. Then, for 2.5 h, the blood glucose level, vascular diameter, heart rate, breath rate, and body temperature were monitored every 5 min. Blood glucose levels were increased from 100 to 400 mg/dL, and then decreased to 300 mg/dL. The arterioles had spontaneously constricted by approximately 5.7 ± 1.1% by 20 min after injection, and then gradually recovered for another 40 min, but the venules did not change. As a control, 10 normal rats were injected with phosphate-buffered saline (PBS), and no constrictions in arterioles were observed. Further, there was good statistical agreement between the changes in arteriolar diameters and blood glucose. Our results present the amount and time of constriction in arterioles, which can potentially help in understanding vascular glucose homeostasis and the relationship between vascular dysfunction and cardiovascular risks.

2. Materials and methods

2.1. High-resolution and high-speed photoacoustic microscopy system

For vascular imaging of the rat's ear, we used a commercial high-speed PAM (OptichoM, Opticho, Republic of Korea) with a water-immersible micro-electro-mechanical systems (MEMS) scanner (Fig. 1a), which provided a lateral resolution of 5 μm and an imaging depth to approximately 1 mm [53]. In operation, 10-nanosecond pulses of light from a 532 nm pulsed laser (AWAVE532–1 W-10 K, Advanced Optowave, NY, USA) were delivered to the PAM through a low-insertion-loss single-mode patch cable (P1–460 P-FC-1, Thorlabs, NJ, USA). On the PAM, a hot mirror (FM02R, Thorlabs, NJ, USA) passed 90% of the light, which was focused on targets to create the PA effect. The generated US waves were returned to the system, detected by a 50-MHz US transducer (V214-BB-RM, Olympus NDT, MA, USA), and acquired by a waveform digitizer card (ATS9350, Alazar Technologies, QC, Canada) with a sampling rate of 500 MHz. Meanwhile, to compensate the acquired PA signals, the 10% of the light reflected by the hot mirror was measured by a photodetector (PDA36A-EC, Thorlabs, NJ, USA), using the waveform digitizer card. The MEMS scanner (OptichoM-MS, Opticho, Republic of Korea) achieved high-speed PA imaging by steering the light and US waves, and two motorized linear stages (L-509, Physik Instrumente, Germany) extended the imaging area. The components were operated and synchronized using a multi-functional data acquisition (DAQ) board (PCIe-6321, National Instruments, TX, USA), and their functionalities were programmed in LabVIEW (National Instruments, TX, USA).

The PAM system provided images of vascular networks in a volume of $4 \times 6 \times 1$ mm^3 (along the X, Y, and Z axes, respectively) within 2 min. The measured optical energy was less than 8 mJ/cm^2, below the 20 mJ/cm^2 maximum permissible exposure (MPE) value for skin set by the American National Standards Institute (ANSI). From the 3D data of the vascular networks, top-view blood vessel images, so called PA maximum amplitude projection (MAP) images, were obtained by projecting the maximum value of the PA signals along the depth direction. The processing and visualization were performed in MATLAB (MathWorks, MA, USA) with the help of 3D Photoacoustic Visualization Studio (PHOVIS) including a scan converter for optical scanning photoacoustic microscopy [54].

2.2. Measurement of heart and breath rates

A custom-made printed circuit board (PCB) for photoplethysmography (PPG) was used to measure the heart and breath rates (Fig. 1a). The PCB consists of a light emitting diode (LED, LVMTG1400, Vishay Semiconductors, PA, USA) and a photodiode (PD, SFH2716. Osram Opto Semiconductors, Germany), and the PPG signals obtained from the PD were collected on the DAQ board at a sampling rate of 100 Hz. The PPG signal acquisition was programmed on the PAM software system, and thus the PPG signals were acquired during each PAM imaging experiment with the PCB installed under the rat's heart. Finally, the heart and breath rates were obtained by extracting the PPG waveform's two fundamental frequencies from its frequency response

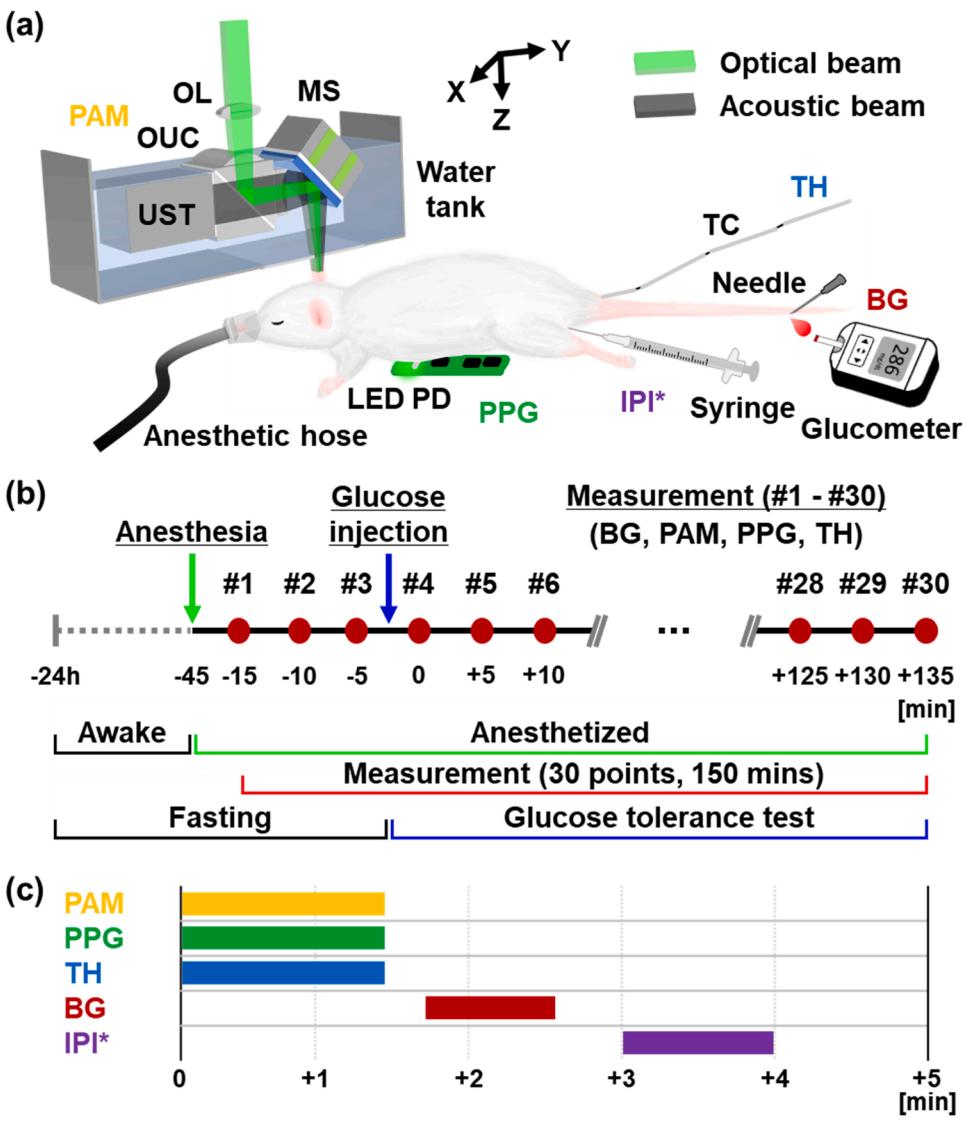

Fig. 1. (a) Graphical representation of the whole system, including photoacoustic microscopy (PAM), photoplethysmography (PPG), thermometry (TH), blood glucose (BG) measurement, and intraperitoneal injection (IPI). (b) Experimental protocol and (c) Time sequence for each measurement. MS, micro-electro-mechanical systems (MEMS) scanner; OL, objective lens; OUC, opto-ultrasound beam combiner; UST, ultrasound transducer; LED, light-emitting diode; PD, photodiode; and TC, thermocouple. * IPI was performed on the third measurement only.

obtained via a fast Fourier transform, which was performed in MATLAB. The faster of the two fundamental frequencies is the heart rate, and the slower is the breath rate.

2.3. Measurement of body temperature

A thermocouple (DH-1–24-K-12, Omega Engineering, CT, USA) was placed in the rat's rectum (Fig. 1a). The rectal temperature was measured using a thermocouple module (NI 9213, National Instruments, TX, USA) and a DAQ chassis (cDAQ-9174, National Instruments, TX, USA) at a sampling rate of 100 Hz. The body temperature measurement was integrated on the PAM software system, and the body temperature was continuously measured during the PA imaging and PPG sensing measurements. Finally, the measured body temperature values were averaged to reduce sensing variance.

2.4. Control and measurement of blood glucose

After the PA vascular image, heart rate, breath rate, and body temperature had been obtained, the rat's tail vein was punctured using a needle and allowed to bleed slightly, then blood glucose levels were measured with a blood glucose meter (Accu-Chek Guide, Roche Diabetes Care, Switzerland) and its strips (Fig. 1a). To increase the fasting blood glucose level, a 20% glucose solution was prepared by mixing dextrose powder (Dextrose, Sigma-Aldrich, MO, USA) and PBS in a ratio of 1:4, using a precision balance (FX-200i, A&D Company, South Korea). Then, 1.5 mL of glucose solution was intraperitoneally injected using a 31-gauge insulin syringe (Ultra-Fine II, Becton, Dickinson and Company, NJ, USA) (Fig. 1a). It had been previously reported that an intraperitoneal injection of 1.5 mL glucose solution commonly raises 6-week-old rats' blood glucose level from 100 mg/dL to 350 mg/dL. The 1.5 mL of 20% glucose solution injected in our experiments is equivalent to 2 g of glucose/kg body weight in the previously reported studies of the intraperitoneal glucose tolerance test (IPGTT) [55,56]. As a control, 1.5 mL of PBS was prepared and injected.

2.5. Experimental procedures

All experimental procedures were performed following a protocol approved by the Institutional Animal Care and Use Committee (IACUC) of the Pohang University of Science and Technology (POSTECH). Twenty Sprague-Dawley rats (6 weeks, ~150 g) were prepared, ten for an experimental group and ten for a control group. The experimental steps and their timing are shown in Fig. 1b. The rat was fasted for 24 h (supplied with water only) and then was anesthetized with a flow of 0.5 L/min O_2 and 2% isoflurane, using a vaporized anesthesia system

(VIP 3000 Veterinary Vaporizer, Midmark, OH, USA). The experiments were conducted only when the rats' blood glucose levels were sufficiently low, about 100 mg/dL. Under respiratory anesthesia, the following parameters were collected every 5 min for 150 min, a total of 30 measurement instances: blood glucose at the tail, vascular images of the ear, heart and respiration rates at the chest, and body temperature in the rectum (Fig. 1b-c). These five parameters were measured 3 times before and 27 times after the intraperitoneal injection of glucose or PBS, respectively. An infrared lamp (Infralux-300A, Daekyung Electro Medical, South Korea) was used to maintain the body temperature during the experiments.

2.6. Postprocessing to measure vascular diameters

To extract the vascular diameters in the PA images, blood vessel segmentation and vascular diameter calculations were sequentially performed in MATLAB (Supplementary Fig. S1). First, blood vessels were enhanced and binarized using a Frangi filter and adaptive thresholding [57]. Then, to exclude tiny blood vessels and salt-and-pepper noise, connected blood vessels were numerically labeled using connected-component labeling, and those components with a small number of pixels were removed. Second, the blood vessels' centerlines were found through image skeletonization, and points where the lines overlapped were removed in advance to avoid possible errors in

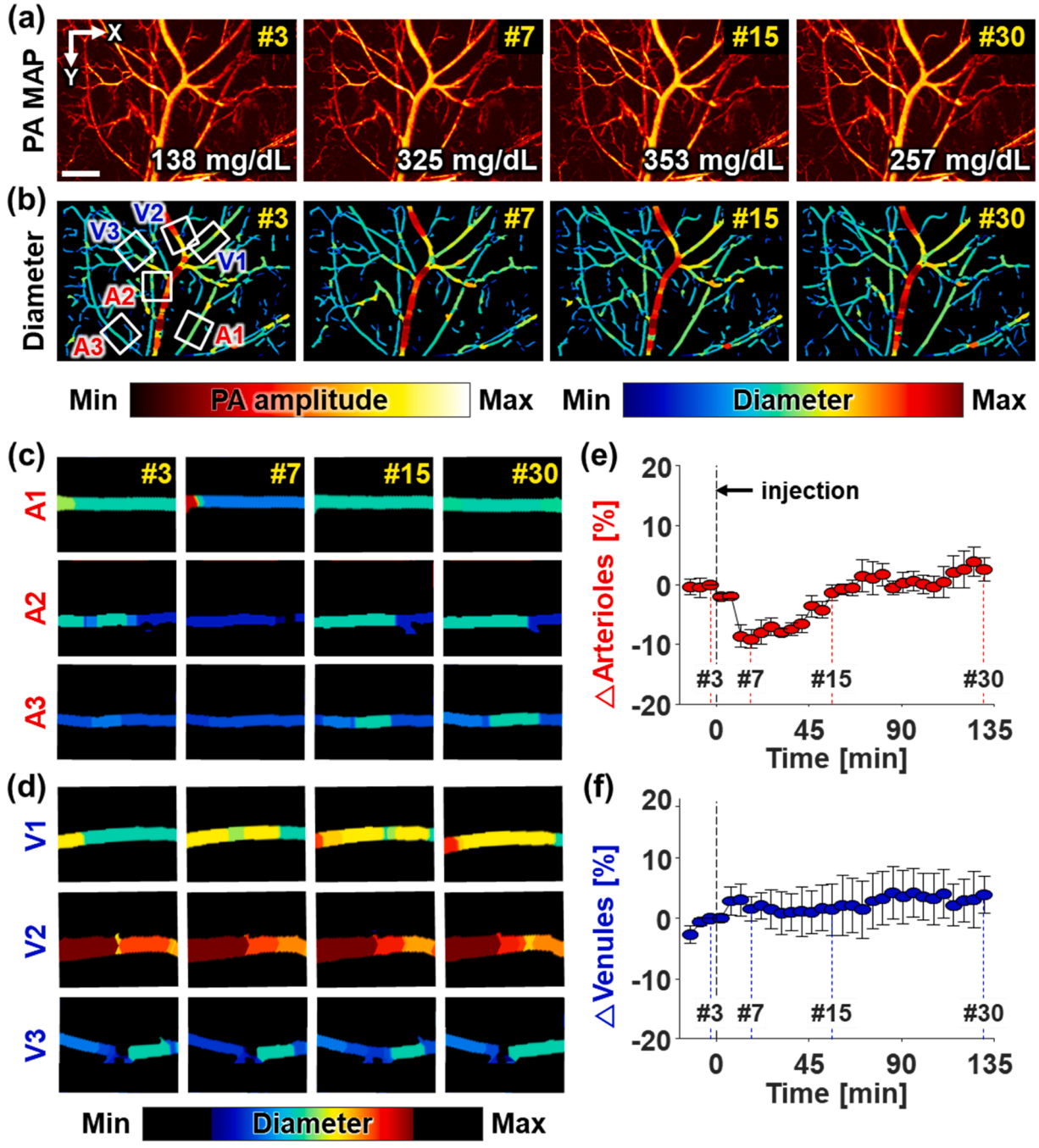

Fig. 2. High-resolution photoacoustic (PA) monitoring of vascular networks during intraperitoneal glucose tolerance testing for 150 min, measured at 5-min intervals. (a) PA maximum amplitude projection (MAP) vascular images, and (b) their diameter-mapped vascular images in the 3rd, 7th, 15th, 30th measurements. Magnified images of (c) 3 arterioles (A1–A3) and (d) 3 venules (V1–V3) in the region of the white boxes in (b). Changes in (e) arteriolar and (f) venular diameters (mean ± standard error). The individual changes in (e–f) are represented in Supplementary Fig. S3. Scale bar: 1 μm.

calculating the diameters. Next, the specific region of interest (e.g., 20 ×20 pixels) for one point was selected, and the minimum distance between this point and the nearest point in non-vascular areas was calculated. The calculated distance corresponds to the blood vessel's radius at the point. By repeating the above calculation for all points on the centerlines, diameter-mapped lines were obtained. Finally, diameter-mapped vascular image was generated in an image form by dilating the diameter-mapped lines and masking it using the segmented blood vessels. The obtained diameters were used only change in diameter with unit of percentage (%) due to an expected error with actual diameters, although subjectivity was excluded by minimizing user interventions.

3. Results

3.1. Time-dependent PA vascular images and serial monitoring of blood glucose level, arteriolar and venular diameters, heart rate, breath rate, and body temperature

After 24-hour fasting, a typical experimental rat's initial blood glucose level was about 100 mg/dL, which remained unchanged until injection. After an intraperitoneal injection of 1.5 mL of glucose solution with a 20% concentration, the blood glucose level rapidly increased, reaching ~400 mg/dL in 40 min, and then gradually decreased to ~300 mg/dL (Supplementary Fig. S2a). In contrast, in the PBS-injected group the blood glucose level remained under 140 mg/dL (Supplementary Fig S2b). The changes in blood glucose levels after injections of glucose and PBS solutions were clearly distinct between the two groups.

During PA imaging for 2.5 h, 30 PA vascular images were acquired

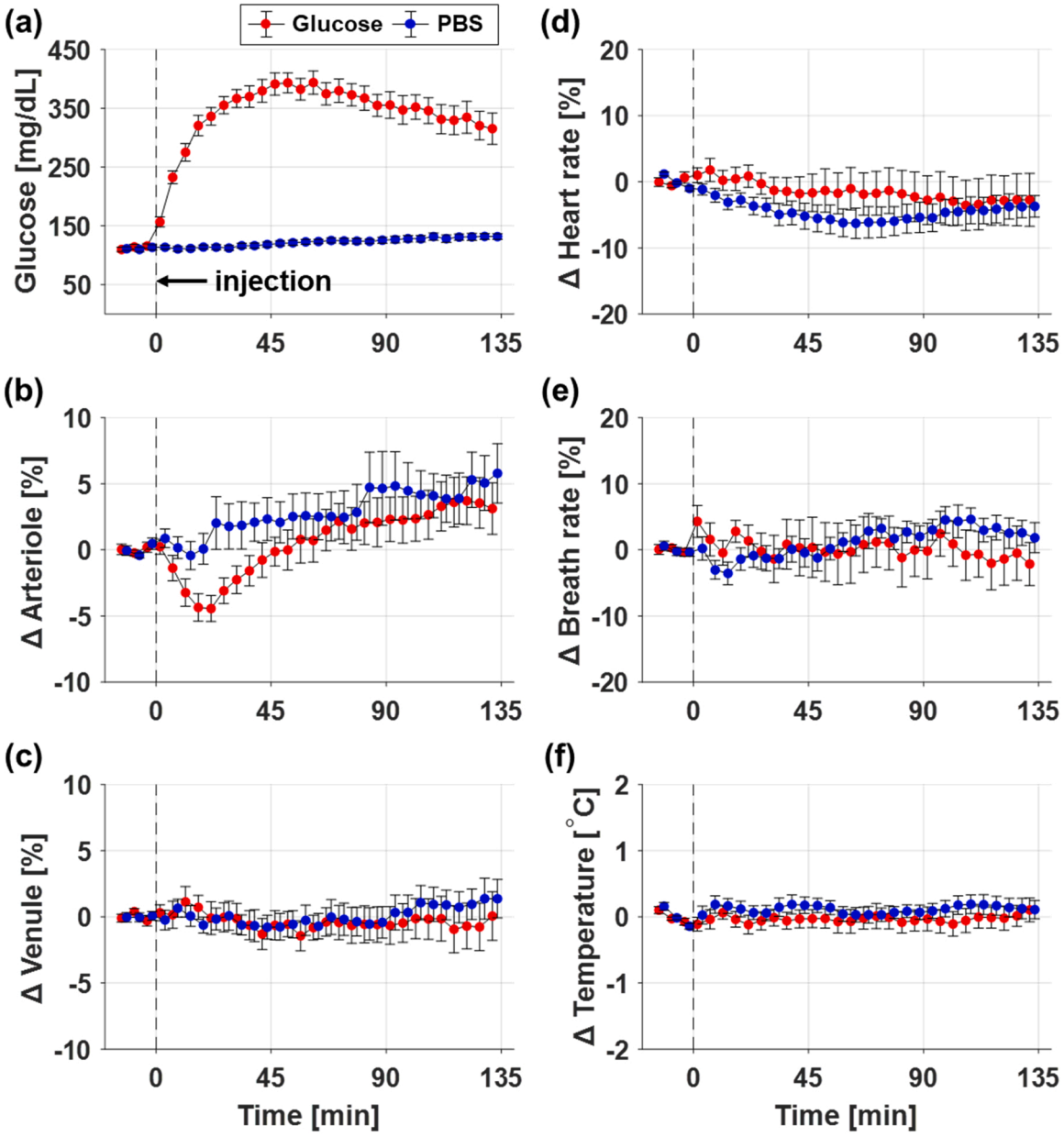

Fig. 3. Time-dependent measurements of (a) blood glucose, (b) arteriolar diameter, (c) venular diameter, (d) heart rate, (e) breath rate, and (f) body temperature (n = 10 for the glucose-injected group, and n = 10 for the PBS-injected group). Each data point and its error bar represent the mean and standard error, respectively. The baselines for each data series are determined by calculating the average of the first three data points before injection.

(Supplementary Movie 1). Among the 30 images, Fig. 2a–b represent the 3rd, 7th, 15th, and 30th PA MAP vascular images and the corresponding diameter-mapped vascular images from one case in the glucose-injected group, and the corresponding blood glucose levels are 138, 325, 353, and 257 mg/dL, respectively. It can be seen that the arterioles constrict in the 7th images and then recover (A1–A3), while the venules exhibit no changes in their diameters (V1-V3). The vasoconstriction and re-vasodilation in the arterioles are more clearly seen in the magnified diameter-mapped vascular images with a narrow colormap range (Fig. 2c–d). To quantify the changes in vascular diameters, three arterioles and three venules were manually selected in the PA vascular images based on the arteriole-venule pair's characteristics that arterioles and venules are arranged side by side in pairs and one venule is relatively larger than the paired arteriole. The baseline of each measurement was calculated by averaging the first, second, and third measurements before injection. The dynamic changes in diameters of single arterioles and venules by normalizing all values of 30 measurements for each blood vessel using its baseline value (Supplementary Fig. S3). Then, the means and standard deviations of arteriolar and venular diameters numerically represented (Fig. 2e–f).

Along with monitoring the blood glucose level and vascular diameters, we also measured other metabolic parameters (e.g., heart rate, breath rate, and body temperature) at the same time point. Fig. 3 shows statistical time-series measurements of those parameters (n = 10 for the glucose-injected group, and n = 10 for the PBS-injected group). The average blood glucose levels for each group are shown in Fig. 3a, where each data point and its error bar represent the mean and standard error, respectively. As soon as the glucose solution is intraperitoneally injected, the blood glucose level rapidly increases, becomes saturated near 393 ± 17 mg/dL within 60 min, and then gradually decreases to 315 ± 27 mg/dL in 135 min. This rising pattern of the blood glucose level indicates acute hyperglycemia and is clearly distinct from the pattern for PBS injection. Fig. 3b–c show the changes in the arteriolar and venular diameters, which were obtained by calculating the mean and standard error of the arteriolar and venular diameters of 10 rats. The changes in arteriolar and venular diameters are obviously different in the glucose- and PBS-injected groups. In the glucose-injected group, the arterioles quickly constrict by about 4.4 ± 0.98% with 20 min after the glucose injection and then gradually recovers. Interestingly, it shows that arterioles constrict when blood glucose rises sharply. On the other hand, in the PBS-injected group, the arterioles do not constrict. The diameters of the venules do not change significantly in either group. Fig. 3d–f show the changes in heart rate, breath rate, and body temperature. The deviations of these metabolic parameters from their baselines are within 10% for the heart rate, 10% for the breath rate, and 0.2 ℃ for the body temperature (Fig. 3d–f). This maintained metabolism indirectly indicates that there are no short-term adverse effects during the rapid rise in blood glucose. Thus, we deduce that these vascular changes are caused by the rapidly rising blood glucose, and not by changes in other metabolic parameters.

The arteriolar diameters become smaller in nine of the ten glucose-injected cases, whereas positive and negative changes were evenly observed in the PBS-injected cases (Supplementary Fig. S4). For the venular diameters, positive and negative changes were evenly distributed in both the glucose and PBS groups (Supplementary Fig. S4). To quantify the changes in the arteriolar and venular diameters, the maximum changes within 30 min after injection of glucose and PBS (red boxes in Supplementary Fig. S4) were quantified, and are represented as the scattered boxplots in Fig. 4a-b. Further, the values of the mean and standard error for the maximum changes in arteriolar diameters are –5.7 ± 1.1% and 1.5 ± 2.3% for glucose and PBS groups, respectively. The p value for the arterioles from Welch's t-test is 0.015, which shows a significant difference between the two groups. However, the maximum changes in venular diameters are 0.6 ± 1.5% and 0.71 ± 1.3% for the glucose and PBS groups, respectively, and the calculated p value of 0.96 indicates no significant difference. These statistics support the inference that the arterioles were constricted when the blood glucose level rose rapidly.

4. Discussion

4.1. Photoacoustic observation of arteriolar vasoconstriction in acute hyperglycemia

The IPGTT created an acute hyperglycemic situation in which blood glucose rapidly rose from 100 to 400 mg/dL. During the 2.5-hour duration of the IPGTT, vascular images and metabolic parameters, including the heart rate, respiration rate, and body temperature, were monitored at 5-min intervals. This diverse biometric information could be simultaneously obtained by adding functions to measure PPG signals and temperature in the PA microscope's software, thus enabling long-term monitoring experiments to be conducted seamlessly.

In the monitoring experiments, acute vasoconstriction was observed only in arterioles when blood glucose rapidly rose. Blood vessels, whose walls consist of layers of vascular smooth muscle, change their diameters in response to different physiological changes, regulating blood flow to appropriately circulate blood to organs [58]. It is widely known that this dynamic changes in vascular diameter occurs are greater in arterioles

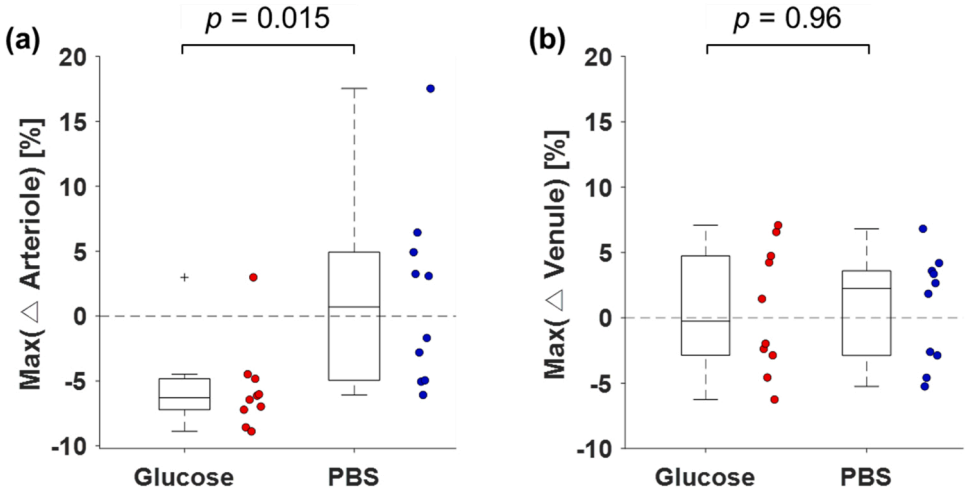

Fig. 4. Maximum vasoconstriction changes in arterioles and venules during rising blood glucose levels for (a) the glucose- and (b) PBS-injected groups. The p values were calculated from the Welch's unequal variance t-test.

compared to venules, because arterioles have more vascular smooth muscle than venules [12]. Thanks to the high-speed and high-resolution of PAM, we could capture acute and small morphological changes in blood vessels and verify the constriction of the arterioles only. Further, our results present the timing and degree of vasoconstriction, whereas a previous study indirectly inferred vasoconstriction from changes in blood flow [59].

4.2. Acute hyperglycemia and endothelial dysfunction

The pancreas maintains the blood glucose level by timely releasing glucagon and insulin [60]. When blood glucose is low, glucagon is released to raise it; conversely, when blood glucose is high, insulin is secreted to lower it. The maintenance of blood glucose level through negative feedback is referred to as glucose homeostasis. When glucose solution is intraperitoneally injected, as in our study, insulin is secreted because glucose is absorbed into blood and raises blood glucose level [61]. However, during acute rapid hyperglycemia, the amount of insulin secreted follows the increase in blood glucose, which may cause momentary hyperinsulinemia [62]. In hyperinsulinemia, insulin acts as a vasoconstrictor by causing endothelial dysfunction [16]. This vasoconstrictive action of insulin from hyperinsulinemia following acute hyperglycemia is consistent with our results (Figs. 2 and 3). Interestingly, the vasoconstriction and the change in blood glucose have similar patterns, with a 15-minute delay (Fig. 5). The physiological link may be that the dynamic insulin secretion rate is controlled by the change in blood glucose [63]. In addition, it has been recently reported that a reinforcement learning-based artificial intelligence (AI) also secreted insulin in response to dynamic changes in blood glucose, but not to static blood glucose [64]. These interconnected results from multiple studies support our opinion that excessive secretion of insulin induced by acute hyperglycemia induces vasoconstriction.

4.3. Limitations of this study

Although our results clearly demonstrate vasoconstriction in acute hyperglycemia, there are limitations. Our experiments were conducted under anesthesia and blood was sampled every 5 min, conditions that may cause physiological changes. The experimental preparation, such as handling and cage transportation, as well as the process of blood sampling can stress the rats and raise their blood glucose level [65]. Those issues could be managed in the near future by continuously monitoring glucose levels [66]. It is inevitable that anesthesia for stable PA imaging affects the results. A previously published study reported that both arteries and veins dilate when isoflurane anesthesia begins [67]. The diameters of arterioles in our results also tended to increase, whereas the venules with no vascular smooth muscles kept almost constant. Even while the arterioles slightly dilate during anesthesia, they constricted at the moment of the acute elevation of blood glucose, indicating the effect on the endothelium by increased blood glucose is greater than by anesthesia. However, because anesthesia affects cardiovascular and respiratory functions [68,69], we excluded the non-injected control group because it did not meet the hypothesis to maintain their heart and breath rates. The 10 rats not supplied with water under prolonged anesthesia became dehydrated due to the lack of water, resulting in 10% drops in their heart rate and breath rate, even though hypothermia was prevented (Supplementary Fig. S5). Due to the unstable heart rate, unexpected changes in arteriolar diameters could be observed, although venules maintained their diameters.

To obtain more meaningful results, it is required to measure an insulin level and analyze the trend of insulin secretion together, although it is a well-known scientific fact that insulin is secreted when blood glucose level rises. In our experimental protocol, it was difficult to measure the insulin level due to temporal and spatial constraints: With the water tank, PPG PCB, and temperature sensor installed, the PA imaging and PPG/temperature/glucose measurements had to be performed within 5 min. In follow-up studies, experiments would be redesigned considering the insulin measurement. In addition, this experiment should be performed on awake rats. However, the ~5% vasoconstriction observed under anesthesia may be too small to capture, due to motion artifacts from the un-anesthetized rats.

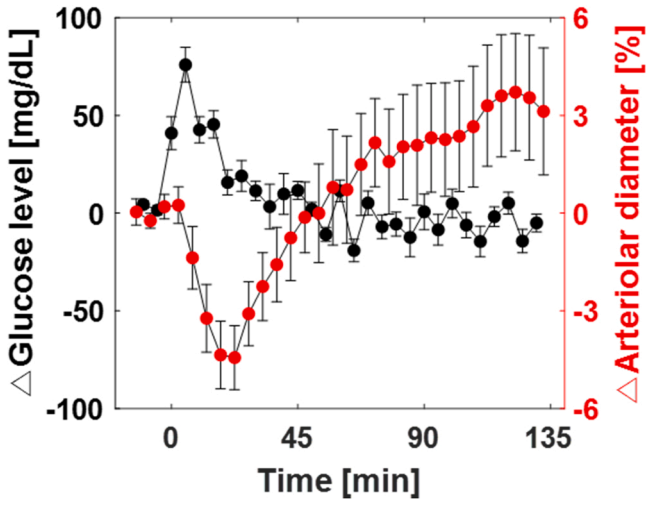

Fig. 5. Relationship between changes in blood glucose and the diameter of arterioles.

4.4. Significance in clinical perspectives

As evidence has been reported that acute rise in blood glucose after a meal increases cardiovascular risks, interest in the management of glucose variability is increasing [70,71]. Accordingly, for the purpose of preventing diabetes, clinical study on PPH in healthy persons has been reported [72]. The study presented that acute hyperglycemia causes endothelial dysfunction even in healthy population. Our results suggest vasoconstriction as another evidence of endothelial dysfunction following acute hyperglycemia in healthy animals. These finding suggest that non-diabetics could also pay attention on consuming too much sugar.

The intuitive presentation of vasoconstriction following PPH shows the potential of PA technique to be used in medical devices and healthcare. However, further technological advances are required for use with humans. Especially, microvascular imaging is vulnerable to motion because high resolution should be provided to visualize small blood vessels. A skin-attachable patch-type PA imaging module could be a solution [73]. If such a device would be developed, it is expected that it could be widely used for various studies on vascular responses.

5. Conclusions

We have monitored vascular diameters in rats during acute hyperglycemia and observed vasoconstriction in arterioles when the blood glucose level rapidly increased after intraperitoneal glucose injection. To the best of our knowledge, and for the first time, high-resolution PA imaging visually captured and quantified vasoconstriction caused by an intrinsic reaction to a rapid increase in blood glucose. The arterioles constricted by about –5.7 ± 1.1% when the blood glucose level rapidly increased from 100 to 350 mg/dL. They recovered as the level saturated at 400 mg/dL and then gradually decreased. During this period, venules, heart rate, breath rate, and body temperature were maintained. These results demonstrated the opposite trends in changes in arteriolar constriction and blood glucose level from transient vasoconstriction produced by acute hyperglycemia. Further, it has been discussed about acute hyperglycemia, hyperinsulinemia, insulin response, and their connections. These results and discussion would help understanding

vascular glucose homeostasis and the relationship between diabetes and cardiovascular diseases.

Declaration of Competing Interest

J. Ahn, J. Y. Kim and C. Kim have financial interests in Opticho, which, however, did not support this work. J. W. Baik was with Pohang University of Science and Technology and is now an employee of Samsung Electronics, Co. Ltd. K. Choi and S. H. Nam are employees of Samsung Electronics, Co. Ltd. S. Park has financial interests in Curestream, which, however, did not support this work. Pohang University of Science and Technology and Samsung Electronics, Co. Ltd. signed a contract to conduct the studies reported here. D. Kim, and S. Lee declare no competing interests.

Data Availability

Data will be made available on request.

Acknowledgements

This study was supported by the Samsung Advanced Institute of Technology; by the Basic Science Research Program through the National Research Foundation of Korea (NRF) funded by the Ministry of Education (2020R1A6A1A03047902) and the Ministry of Science and ICT (2023R1A2C3004880); by the National Research and Development Program through the NRF funded by Ministry of Science and ICT (2021M3C1C3097619); by the Korea Medical Device Development Fund grant funded by the Korea Government (the Ministry of Science and ICT, the Ministry of Trade, Industry and Energy, the Ministry of Health & Welfare, the Ministry of Food and Drug Safety) (9991007019, KMDF_PR_20200901_0008); and by the BK21 FOUR project.

Appendix A. Supporting information

Supplementary data associated with this article can be found in the online version at doi:10.1016/j.pacs.2023.100485.

References

[1] A. Ceriello, Cardiovascular effects of acute hyperglycaemia: pathophysiological underpinnings, Diabetes Vasc. Dis. Res. 5 (4) (2008) 260–268.
[2] B.M. Leon, T.M. Maddox, Diabetes and cardiovascular disease: epidemiology, biological mechanisms, treatment recommendations and future research, World J. Diabetes 6 (13) (2015) 1246–1258.
[3] A.S.D.M. Matheus, L.R.M. Tannus, R.A. Cobas, C.C.S. Palma, C.A. Negrato, M.D. B. Gomes, Impact of diabetes on cardiovascular disease: an update, Int. J. Hypertens. 2013 (2013), 653789.
[4] K. Node, T. Inoue, Postprandial hyperglycemia as an etiological factor in vascular failure, Cardiovasc. Diabetol. 8 (1) (2009) 23.
[5] E. Mah, R.S. Bruno, Postprandial hyperglycemia on vascular endothelial function: mechanisms and consequences, Nutr. Res. 32 (10) (2012) 727–740.
[6] R. Marfella, G. Verrazzo, R. Acampora, C. La Marca, R. Giunta, C. Lucarelli, G. Paolisso, A. Ceriello, D. Giugliano, Glutathione reverses systemic hemodynamic changes induced by acute hyperglycemia in healthy subjects, Am. J. Physiol. Endocrinol. Metab. 268 (6) (1995) E1167–E1173.
[7] D. Giugliano, R. Marfella, L. Coppola, G. Verrazzo, R. Acampora, R. Giunta, F. Nappo, C. Lucarelli, F. D'Onofrio, Vascular effects of acute hyperglycemia in humans are reversed by l-arginine, Circulation 95 (7) (1997) 1783–1790.
[8] R. Marfella, F. Nappo, L. De Angelis, M. Siniscalchi, F. Rossi, D. Giugliano, The effect of acute hyperglycaemia on QTc duration in healthy man, Diabetologia 43 (5) (2000) 571–575.
[9] P.N. Båvenholm, S. Efendic, Postprandial hyperglycaemia and vascular damage - the benefits of acarbose, Diabetes Vasc. Dis. Res. 3 (2) (2006) 72–79.
[10] T. Sakamoto, H. Ogawa, H. Kawano, N. Hirai, S. Miyamoto, K. Takazoe, H. Soejima, K. Kugiyama, M. Yoshimura, H. Yasue, Rapid change of platelet aggregability in acute hyperglycemia: detection by a novel laser-light scattering method, Thromb. Haemost. 83 (2000) 475–479.
[11] A. Ceriello, K. Esposito, L. Piconi, M.A. Ihnat, J.E. Thorpe, R. Testa, M. Boemi, D. Giugliano, Oscillating glucose is more deleterious to endothelial function and oxidative stress than mean glucose in normal and type 2 diabetic patients, Diabetes 57 (5) (2008) 1349.
[12] L.A. Martinez-Lemus, The dynamic structure of arterioles, Basic Clin. Pharmacol. Toxicol. 110 (1) (2012) 5–11.
[13] D. Alonso, M.W. Radomski, The nitric oxide-endothelin-1 connection, Heart Fail. Rev. 8 (1) (2003) 107–115.
[14] C. Cardillo, S.S. Nambi, C.M. Kilcoyne, W.K. Choucair, A. Katz, M.J. Quon, J. A. Panza, Insulin stimulates both endothelin and nitric oxide activity in the human forearm, Circulation 100 (8) (1999) 820–825.
[15] C.A. Meza, J.D. La Favor, D.-H. Kim, R.C. Hickner, Endothelial dysfunction: is there a hyperglycemia-induced imbalance of NOX and NOS? Int J. Mol. Sci. 20 (15) (2019) 3775.
[16] M.A. Potenza, F. Addabbo, M. Montagnani, Vascular actions of insulin with implications for endothelial dysfunction, Am. J. Physiol. -Endocrinol. Metab. 297 (3) (2009) E568–E577.
[17] G. Ahlborg, J. Lindström, Insulin sensitivity and big ET-1 conversion to ET-1 after ETA- or ETB-receptor blockade in humans, J. Appl. Physiol. 93 (6) (2002) 2112–2121.
[18] V. Ormazabal, S. Nair, O. Elfeky, C. Aguayo, C. Salomon, F.A. Zuñiga, Association between insulin resistance and the development of cardiovascular disease, Cardiovasc. Diabetol. 17 (1) (2018) 122.
[19] B.C. Bucca, D.M. Maahs, J.K. Snell-Bergeon, J. Hokanson, S. Rinella, F. Bishop, A. Boufard, J. Homann, C.Y. Cheung, T.Y. Wong, Dynamic changes in retinal vessel diameter during acute hyperglycemia in type 1 diabetes, J. Diabetes Complicat. 32 (2) (2018) 234–239.
[20] P. Kappelgaard, S.K. Holfort, O.N. Klefter, M. Larsen, Retinal vessel diameter changes in relation to dark adaptation and acute hyperglycemia, J. Ophthalmol. 2018 (2018), 7064359.
[21] C.C. Kwan, H.E. Lee, G. Schwartz, A.A. Fawzi, Acute hyperglycemia reverses neurovascular coupling during dark to light adaptation in healthy subjects on optical coherence tomography angiography, Invest Ophthalmol. Vis. Sci. 61 (4) (2020) 38.
[22] I.C. Holmen, S.M. Konda, J.W. Pak, K.W. McDaniel, B. Blodi, K.E. Stepien, A. Domalpally, Prevalence and severity of artifacts in optical coherence tomographic angiograms, JAMA Ophthalmol. 138 (2) (2020) 119–126.
[23] X. Yao, M. Ke, Y. Ho, E. Lin, D.W.K. Wong, B. Tan, L. Schmetterer, J. Chua, Comparison of retinal vessel diameter measurements from swept-source OCT angiography and adaptive optics ophthalmoscope, Br. J. Ophthalmol. 105 (3) (2021) 426.
[24] T. von Hanno, A.K. Sjølie, E.B. Mathiesen, Retinal vascular calibre and response to light exposure and serial imaging, Acta Ophthalmol. 92 (5) (2014) 444–448.
[25] W. Zhen, L. Weihua, L. Pengcheng, Q. Jianjun, L. Qingming, Acute hyperglycemia compromises cerebral blood flow following cortical spreading depression in rats monitored by laser speckle imaging, J. Biomed. Opt. 13 (6) (2008) 1–6.
[26] A. Peretz, D.F. Leotta, J.H. Sullivan, C.A. Trenga, F.N. Sands, M.R. Aulet, M. Paun, E.A. Gill, J.D. Kaufman, Flow mediated dilation of the brachial artery: an investigation of methods requiring further standardization, BMC Cardiovasc. Disord. 7 (1) (2007) 11.
[27] L. Nie, D. Xing, S. Yang, In vivo detection and imaging of low-density foreign body with microwave-induced thermoacoustic tomography, Med. Phys. 36 (8) (2009) 3429–3437.
[28] S. Jeon, J. Kim, D. Lee, J.W. Baik, C. Kim, Review on practical photoacoustic microscopy, Photoacoustics 15 (2019), 100141.
[29] J. Xia, J. Yao, L.V. Wang, Photoacoustic tomography: principles and advances, Electro Waves (Camb.) 147 (2014) 1–22.
[30] J.W. Baik, H. Kim, M. Son, J. Choi, K.G. Kim, J.H. Baek, Y.H. Park, J. An, H.Y. Choi, S.Y. Ryu, J.Y. Kim, K. Byun, C. Kim, Intraoperative label-free photoacoustic histopathology of clinical specimens, Laser Photonics Rev. 15 (10) (2021), 2100124.
[31] J. Kim, B. Park, J. Ha, I. Steinberg, S.M. Hooper, C. Jeong, E.-Y. Park, W. Choi, T. Liang, J.S. Bae, R. Managuli, Y. Kim, S.S. Gambhir, D.-J. Lim, C. Kim, Multiparametric photoacoustic analysis of human thyroid cancers in vivo, Cancer Res. 81 (18) (2021) 4849.
[32] H. Kim, J.W. Baik, S. Jeon, J.Y. Kim, C. Kim, PAExM: label-free hyper-resolution photoacoustic expansion microscopy, Opt. Lett. 45 (24) (2020) 6755–6758.
[33] M. Chen, X. Duan, B. Lan, T. Vu, X. Zhu, Q. Rong, W. Yang, U. Hoffmann, J. Zou, J. Yao, High-speed functional photoacoustic microscopy using a water-immersible two-axis torsion-bending scanner, Photoacoustics 24 (2021), 100309.
[34] J. Ahn, J.W. Baik, Y. Kim, K. Choi, J. Park, H. Kim, J.Y. Kim, H.H. Kim, S.H. Nam, C. Kim, Fully integrated photoacoustic microscopy and photoplethysmography of human in vivo, Photoacoustics 27 (2022), 100374.
[35] J.W. Baik, J.Y. Kim, S. Cho, S. Choi, J. Kim, C. Kim, Super wide-field photoacoustic microscopy of animals and humans in vivo, IEEE Trans. Med. Imaging 39 (4) (2020) 975–984.
[36] J. Park, B. Park, Y. Kim Tae, S. Jung, J. Choi Woo, J. Ahn, H. Yoon Dong, J. Kim, S. Jeon, D. Lee, U. Yong, J. Jang, J. Kim Won, K. Kim Hong, U. Jeong, H. Kim Hyung, C. Kim, Quadruple ultrasound, photoacoustic, optical coherence, and fluorescence fusion imaging with a transparent ultrasound transducer, Proc. Natl. Acad. Sci. 118 (11) (2021), e1920879118.
[37] W. Choi, B. Park, S. Choi, D. Oh, J. Kim, C. Kim, Recent advances in contrast-enhanced photoacoustic imaging: overcoming the physical and practical challenges, Chem. Rev. (2023).
[38] J. Kim, G. Kim, L. Li, P. Zhang, J.Y. Kim, Y. Kim, H.H. Kim, L.V. Wang, S. Lee, C. Kim, Deep learning acceleration of multiscale superresolution localization photoacoustic imaging, Light.: Sci. Appl. 11 (1) (2022) 131.
[39] Z. Qu, C. Liu, J. Zhu, Y. Zhang, Y. Zhou, L. Wang, Two-step proximal gradient descent algorithm for photoacoustic signal unmixing, Photoacoustics 27 (2022), 100379.

[40] W. Choi, E.-Y. Park, S. Jeon, Y. Yang, B. Park, J. Ahn, S. Cho, C. Lee, D.-K. Seo, J.-H. Cho, C. Kim, Three-dimensional Multistructural quantitative photoacoustic and US imaging of human feet in Vivo, Radiology 303 (2) (2022) 467–473.
[41] J. Kim, J. Ahn, G. Kang, J.H. Hwang, C. Kim, High-resolution photoacoustic/ultrasound imaging of the porcine stomach wall: an ex vivo feasibility study, Biomed. Opt. Express 12 (11) (2021) 6717–6729.
[42] J. Lv, Y. Xu, L. Xu, L. Nie, Quantitative functional evaluation of liver fibrosis in mice with dynamic contrast-enhanced photoacoustic imaging, Radiology 300 (1) (2021) 89–97.
[43] G. Huang, J. Lv, Y. He, J. Yang, L. Zeng, L. Nie, In vivo quantitative photoacoustic evaluation of the liver and kidney pathology in tyrosinemia, Photoacoustics 28 (2022), 100410.
[44] S. Choi, J. Yang, S.Y. Lee, J. Kim, J. Lee, W.J. Kim, S. Lee, C. Kim, Deep learning enhances multiparametric dynamic volumetric photoacoustic computed tomography In Vivo (DL-PACT), Adv. Sci. 10 (1) (2023), 2202089.
[45] K. Arie, W. Lidai, Y. Junjie, V.W. Lihong, Functional photoacoustic microscopy of diabetic vasculature, J. Biomed. Opt. 17 (6) (2012) 1–4.
[46] M. Mohesh, B. Renzhe, K. Jin Young, B. Ghayathri, K. Chulhong, C.O. Malini, High-speed simultaneous multiscale photoacoustic microscopy, J. Biomed. Opt. 24 (8) (2019), 086001.
[47] R. Shintate, T. Ishii, J. Ahn, J.Y. Kim, C. Kim, Y. Saijo, High-speed optical resolution photoacoustic microscopy with MEMS scanner using a novel and simple distortion correction method, Sci. Rep. 12 (1) (2022) 9221.
[48] J. Kim, J.Y. Kim, S. Jeon, J.W. Baik, S.H. Cho, C. Kim, Super-resolution localization photoacoustic microscopy using intrinsic red blood cells as contrast absorbers, Light.: Sci. Appl. 8 (1) (2019) 103.
[49] K. Wang, C. Li, R. Chen, J. Shi, Recent advances in high-speed photoacoustic microscopy, Photoacoustics 24 (2021), 100294.
[50] S.-W. Cho, S.M. Park, B. Park, D.Y. Kim, T.G. Lee, B.-M. Kim, C. Kim, J. Kim, S.-W. Lee, C.-S. Kim, High-speed photoacoustic microscopy: a review dedicated on light sources, Photoacoustics 24 (2021), 100291.
[51] H. Kim, J.Y. Kim, S. Cho, J. Ahn, Y. Kim, H. Kim, C. Kim, Performance comparison of high-speed photoacoustic microscopy: opto-ultrasound combiner versus ring-shaped ultrasound transducer, Biomed. Eng. Lett. 12 (2) (2022) 147–153.
[52] Z. Xu, Y. Pan, N. Chen, S. Zeng, L. Liu, R. Gao, J. Zhang, C. Fang, L. Song, C. Liu, Visualizing tumor angiogenesis and boundary with polygon-scanning multiscale photoacoustic microscopy, Photoacoustics 26 (2022), 100342.
[53] J. Ahn, J.Y. Kim, W. Choi, C. Kim, High-resolution functional photoacoustic monitoring of vascular dynamics in human fingers, Photoacoustics 23 (2021), 100282.
[54] S. Cho, J. Baik, R. Managuli, C. Kim, 3D PHOVIS: 3D photoacoustic visualization studio, Photoacoustics 18 (2020), 100168.
[55] M.S. Jørgensen, K.S. Tornqvist, H. Hvid, Calculation of glucose dose for intraperitoneal glucose tolerance tests in lean and obese mice, J. Am. Assoc. Lab Anim. Sci. 56 (1) (2017) 95–97.
[56] S. Andrikopoulos, A.R. Blair, N. Deluca, B.C. Fam, J. Proietto, Evaluating the glucose tolerance test in mice, Am. J. Physiol. -Endocrinol. Metab. 295 (6) (2008) E1323–E1332.
[57] A.F. Frangi, W.J. Niessen, K.L. Vincken, M.A. Viergever, Multiscale vessel enhancement filtering, in: W.M. Wells, A. Colchester, S. Delp (Eds.), Medical Image Computing and Computer-Assisted Intervention — MICCAI'98, Springer, Berlin Heidelberg, Berlin, Heidelberg, 1998, pp. 130–137.
[58] A. Bit, J.S. Suri, A. Ranjani, Anatomy and physiology of blood vessels, Flow Dynamics and Tissue Engineering of Blood Vessels, IOP Publishing, 2020, pp. 1-1-1-16.
[59] F. Markos, C.M. Shortt, D. Edge, T. Ruane-O'Hora, M.I. Noble, Immediate direct peripheral vasoconstriction in response to hyperinsulinemia and metformin in the anesthetized pig, Physiol. Res. 63 (5) (2014) 559–566.
[60] P.V. Röder, B. Wu, Y. Liu, W. Han, Pancreatic regulation of glucose homeostasis, Exp. Mol. Med. 48 (3) (2016) e219-e219.
[61] S. Pilon, A.C. Holloway, E.M. Thomson, Metabolic, stress, and inflammatory biomarker responses to glucose administration in Fischer-344 rats: intraperitoneal vs. oral delivery, J. Pharmacol. Toxicol. Methods 90 (2018) 1–6.
[62] E. Toschi, S. Camastra, A.M. Sironi, A. Masoni, A. Gastaldelli, A. Mari, E. Ferrannini, A. Natali, Effect of acute hyperglycemia on insulin secretion in humans, Diabetes 51 (suppl 1) (2002) S130.
[63] M.G. Pedersen, G.M. Toffolo, C. Cobelli, Cellular modeling: insight into oral minimal models of insulin secretion, Am. J. Physiol. -Endocrinol. Metab. 298 (3) (2009) E597–E601.
[64] S. Lee, J. Kim, S.W. Park, S.M. Jin, S.M. Park, Toward a fully automated artificial pancreas system using a bioinspired reinforcement learning design: in silico validation, IEEE J. Biomed. Health Inform. 25 (2) (2021) 536–546.
[65] H. Tabata, T. Kitamura, N. Nagamatsu, Comparison of effects of restraint, cage transportation, anaesthesia and repeated bleeding on plasma glucose levels between mice and rats, Lab. Anim. 32 (2) (1998) 143–148.
[66] R. Aronson, A. Abitbol, K.S. Tweden, First assessment of the performance of an implantable continuous glucose monitoring system through 180 days in a primarily adolescent population with type 1 diabetes, Diabetes, Obes. Metab. 21 (7) (2019) 1689–1694.
[67] C.T. Sullender, L.M. Richards, F. He, L. Luan, A.K. Dunn, Dynamics of isoflurane-induced vasodilation and blood flow of cerebral vasculature revealed by multi-exposure speckle imaging, J. Neurosci. Methods 366 (2022), 109434.
[68] M.S. McKinney, J.P.H. Fee, R.S.J. Clarke, Cardiovascular effects of isoflurane and halothane in young and elderly adult patients, Br. J. Anaesth. 71 (5) (1993) 696–701.
[69] C.-F. Yang, M. Yu-Chih Chen, T.-I. Chen, C.-F. Cheng, Dose-dependent effects of isoflurane on cardiovascular function in rats, Tzu Chi Med. J. 26 (3) (2014) 119–122.
[70] S. Suh, J.H. Kim, Glycemic variability: how do we measure it and why is it important? Diabetes Metab. J. 39 (4) (2015) 273–282.
[71] E. Standl, O. Schnell, A. Ceriello, Postprandial hyperglycemia and glycemic variability: should we care? Diabetes Care 34 (Supplement_2) (2011) S120–S127.
[72] J. Loader, C. Meziat, R. Watts, C. Lorenzen, D. Sigaudo-Roussel, S. Stewart, C. Reboul, G. Meyer, G. Walther, Effects of sugar-sweetened beverage consumption on microvascular and macrovascular function in a healthy population, Arterioscler., Thromb., Vasc. Biol. 37 (6) (2017) 1250–1260.
[73] X. Gao, X. Chen, H. Hu, X. Wang, W. Yue, J. Mu, Z. Lou, R. Zhang, K. Shi, X. Chen, M. Lin, B. Qi, S. Zhou, C. Lu, Y. Gu, X. Yang, H. Ding, Y. Zhu, H. Huang, Y. Ma, M. Li, A. Mishra, J. Wang, S. Xu, A photoacoustic patch for three-dimensional imaging of hemoglobin and core temperature, Nat. Commun. 13 (1) (2022) 7757.

Joongho Ahn received his B.S degree in Electronics Engineering at Kyungpook National University, South Korea, in 2016, and did the Ph.D. degree in Convergence IT Engineering at Pohang University of Science and Technology (POSTECH), South Korea, in 2022. He worked as a Postdoctoral Research Associate in the Department of Convergence IT Engineering at POSTECH and is currently a Research Assistant Professor of the Department of Convergence IT Engineering at POSTECH. His research interests include the development of ultrasound and photoacoustic imaging systems, and their translational research and commercialization.

Jin Woo Baik received the B.S in Electrical Engineering at Pohang University of Science and Technology (POSTECH) and the Ph.D. degree in the Department of Convergence IT Engineering at POSTECH. In 2022, he joined Samsung Electronics Co., Ltd as a research staff engineer. He has experienced photoacoustic imaging systems integrated with other imaging techniques and image processing for preclinical and clinical applications

Donggyu Kim received his B.S. degree in Mechanical Engineering from the Pohang University of Science and Technology (POSTECH), Republic of Korea, in 2021. He is currently pursuing a Ph.D. degree (M.S.-Ph.D. joint program) in Convergence IT Engineering at POSTECH. His research interests include the development of transparent ultrasound transducer and novel biomedical imaging techniques including photoacoustic microscopy and ultrasound imaging.

Karam Choi received the Ph.D. degree in Interdisciplinary Program in Bioengineering from Seoul National University. She has been a Staff Researcher at Samsung Advanced Institute of Technology since 2017. Her research interests include biomedical signal processing, machine learning and statistical data analysis for healthcare applications.

Seunghyun Lee received the B.S. degree in Electrical and Electronics Engineering from Kyungpook National University, South Korea in 2014. He is currently pursuing the Ph.D. degree (M.S. and Ph.D. joint program) with the Department of Convergence IT Engineering, Pohang University of Science and Technology (POSTECH), South Korea, under the supervision of Prof. Sung-Min Park. His main research interest includes personalized diabetes treatment through artificial intelligence.

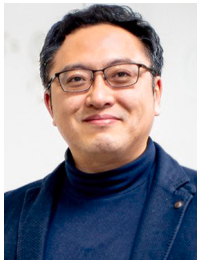

Sung-Min Park received the B.S. and Ph.D. degrees in electrical and computer engineering from Purdue University, West Lafayette, IN, USA, in 2001 and 2006, respectively. From 2006 to 2014, he was with Medtronic, Minneapolis, MN, USA, as the Research and Development Manager, leading an Award-Wining Team in developing the world first MRI conditional pacemaker. From 2014 to 2016, he was with Samsung, Suwon, South Korea, as the Director, spearheading healthcare centric mobile device and mobile health service platform development projects. He is currently a Professor with the Department of Convergence IT Engineering and Electrical Engineering, Pohang University of Science and Technology (POSTECH), Pohang, South Korea, where he has been with since 2016. His current research interests include developing implantable medical device, artificial pancreas systems, digital healthcare, and AI-based closed loop algorithm.

Jin Young Kim received his Ph.D. degree and post-doctoral training from the Departments of Mechanical Engineering and Convergence IT Engineering at Pohang University of Science and Technology (POSTECH), Republic of Korea. He is currently a Research Assistant Professor in the Department of Convergent IT Engineering at POSTECH, working on novel photoacoustic imaging, and multimodal optical imaging systems, and their clinical applications and translations.

Sung Hyun Nam is a VP of technology (Master) at Samsung Advanced Institute of Technology and is developing mobile healthcare related technologies. He finished his Ph.D. in Electrical Engineering at Pennsylvania State University and worked as a postdoctoral research associate at University of California, Berkeley and Los Alamos National Laboratory to study nanoscale photonics. His research interests include various photonics-based sensing applications and non-invasive health sensing technologies.

Chulhong Kim earned his Ph.D. degree and did postdoctoral training at Washington University in St. Louis, Missouri. He currently holds the Young Distinguished Professorship and Mueunjae Chair Professorship, and is a Professor of Convergence IT Engineering, Electrical Engineering, Mechanical Engineering, and Medical Device Innovation Center at Pohang University of Science and Technology in the Republic of Korea. He has received a 2017 IEEE EMBS Early Career Achievement Award, the 2017 Korean Academy of Science and Technology Young Scientist Award, the 2016 Nightingale Award from IFMBE, and the 2017 KOSOMBE Young Investigator Award for "Contributions to multi-scale photoacoustic imaging, ranging from super-resolution atomic force photoactivated microscopy for research to systems for clinical applications."